Published in final edited form as:
IEEE Int Conf Robot Autom. 2013 May 10; 2013: 5390–5395. doi:10.1109/ICRA.2013.6631350.

Implicit Active Constraints for Robot-Assisted Arthroscopy

Edoardo Lopez, **Ka-Wai Kwok**, **Christopher J. Payne**, **Petros Giataganas**, and **Guang-Zhong Yang [Fellow, IEEE]**
Hamlyn Centre for Robotic Surgery, Imperial College London, SW7 2AZ, London, UK

Abstract

This paper presents an *Implicit Active Constraints* control framework for robot-assisted minimally invasive surgery. It extends on current frameworks by prescribing the external constraints implicitly from the operator motion, forgoing the need for pre-operative imaging; the constraints are defined *in situ* so as to avoid the use of invasive fiducial markers.

A *hands-on* cooperatively-controlled robotic platform, comprising of a surgical instrument and a compliant manipulator, has been designed for an arthroscopic procedure. The surgical platform is capable of constraining the pose of the instrument so as to ensure it passes through the incision point and does not cause trauma to the surrounding tissue.

A flexible arthroscopic instrument is designed and its use is investigated to enlarge reachable and dexterous workspace, increasing the accessibility to the target anatomy.

The behaviour of the flexible instrument is analysed. A detailed performance analysis is conducted on a group of subjects for validating the control framework, simulating a minimally invasive arthroscopic procedure. Results demonstrate a statistically significant enhancement in the control ergonomics as well as the accuracy and safety of the procedure.

I. Introduction

Robot Assisted Surgery is playing an important role in improving current surgical practice in terms of precision and safety. In the last decade, the concept of Virtual Fixtures (VFs) [1] and Active Constraints [2] have drawn significant research attention to cooperatively-controlled robotic platforms including *hands-on* robots such as the Acrobot (now acquired by Stanmore Implants, UK, and marketed as Sculptor RGA), the JHU Steady-Hand robot [3] and the MAKOplasty (MAKO Surgical Corp., FL, USA). In cooperatively-controlled systems, the operator and robotic manipulator hold the surgical tool together, this allows for haptic interaction during surgical tasks [4]. Collaborative robotic systems allow the surgeon to remain at the patientside and can be seamlessly introduced into the surgical workflow.

The objective of Active Constraints is to provide effective *in situ* guidance of the surgical tool so as to allow safe access to the target anatomy without causing inadvertent damage to

edoardo.lopez11@imperial.ac.uk

Europe PMC Funders Author Manuscripts

the surrounding anatomy [5]. This is particularly useful for surgical operations that are conducted within a confined workspace [3].

The systems reviewed thus far require pre-acquisition of medical images, such as CT, in order to prescribe the forbidden or “no-go” regions of the anatomy. However, the acquisition of radiological images exposes the patient to radiation and the acquired images have to be laboriously manually segmented to create a patient-specific model. Additionally, the use of medical imaging for some orthopaedic procedures, such as arthroscopy, is not clinically effective. Arthroscopy is a form of revisional surgery and has to be cost-effective. Arthroscopic chondroplasty is a common treatment of early-stage osteoarthritis, which is a disease affecting over 10 million people alone in the UK, costing the country £5.7 billion [6]. In this procedure, the articular surface is accessed through a small incision and the part of joint cartilage is removed, either mechanically or by using laser light [7]. Although the benefits of introducing flexible instruments for arthroscopy have been reported [8]-[10], rigid arthroscopic instruments are adopted in current clinical practice. Without sufficient degrees-of-freedom (DoFs) of the elongated rigid instrument, dexterous workspace is highly restricted.

During arthroscopy, an incision is made to facilitate the passing of instrumentation into the confined joint cavity. The manipulation of interventional tools through an incision point is a common requirement in minimally invasive surgery (MIS) and poses significant challenges to the clinician. The direction of external motion is inverted due to the “fulcrum effect”, this deteriorates hand-eye coordination, especially during the manipulation inside the very limited workspace [11]. In the application of robotics to MIS, researchers have developed mechanically-constrained remote centre of motion (RCM) mechanisms that can manipulate surgical instrumentation about the incision point without causing lateral motion [12]-[16]. In addition to these mechanisms intended for tele-operated systems, a RCM mechanism was proposed for a hands-on cooperatively-controlled robotic platform [17].

The application of software constraints to robotic manipulators to provide a RCM has also been proposed [18]-[20]. These constraints can be programmed so as to allow simple reconfiguration of the incision point and tool orientation, ensuring minimal interference to the surgical workflow. Whilst RCM software constraints are well stablished in tele-operated robotic platforms, such as the DLR MicroSurge platform [21], they have not been applied to co-operatively-controlled hands-on robotic systems.

To this end, we have developed a control framework of Implicit Active Constraints, which does not require the use of medical imaging, but instead the operator is able to prescribe a safe manipulation margin intra-operatively. Under this framework, we first propose software RCM constraints, which can be incorporated into a hands-on cooperatively controlled platform. The system provides the operator with haptic interaction for the safe manipulation of an arthroscopic instrument inside the confined joint cavity. Finally, we also investigated how a flexible instrument can enhance the dexterity and accessibility to the target anatomy. To quantify the practical value of the proposed framework, subject tests were conducted in a simulated arthroscopic chondroplasty task.

II. Methods

A. Generic prescription of Implicit Active Constraints

The haptic constraint to be defined is a surface offset from the articular cartilage surface that allows the instrument tool tip to move freely tangentially across the surface but to be constrained in the normal direction. This anatomical constraint is defined using a few control points obtained by the operators manoeuvring of the instrument tip over the articular cartilage surface, through the incision port. A surface interpolation method, Approximation Based on Smoothing (ABOS) [22], is then used for fitting the control points to a 2D grid. The ABOS method requires bijection between the points and the grid. Due to the anatomical morphology of the articular surface, it has been assumed that at least one plane will exist whereby a grid can be defined for preserving bijection.

In our extended version of ABOS (eABOS), we use the *multiple regression* technique [23] to evaluates the plane $z = a \cdot x + b \cdot y + c$ that best interpolates all the points.

In considering three arbitrary points $\boldsymbol{Q}_1 = [0; 0; c]^T$, $\boldsymbol{Q}_2 = [1; 0; a + c]^T$ and $\boldsymbol{Q}_3 = [0; 1; b + c]^T$ on the plane, the reference frame $\{\hat{0}\} = (\hat{\boldsymbol{x}}, \hat{\boldsymbol{y}}, \hat{\boldsymbol{z}})$ can be defined, with $\hat{\boldsymbol{x}}$ and $\hat{\boldsymbol{y}}$ lying on the plane[1]:

$$\hat{\boldsymbol{x}} = \frac{\overrightarrow{\boldsymbol{Q}_1\boldsymbol{Q}_2}}{||\overrightarrow{\boldsymbol{Q}_1\boldsymbol{Q}_2}||} \quad \hat{\boldsymbol{z}} = \frac{\overrightarrow{\boldsymbol{Q}_1\boldsymbol{Q}_2} \times \overrightarrow{\boldsymbol{Q}_1\boldsymbol{Q}_3}}{||\overrightarrow{\boldsymbol{Q}_1\boldsymbol{Q}_2} \times \overrightarrow{\boldsymbol{Q}_1\boldsymbol{Q}_3}||} \quad \hat{\boldsymbol{y}} = \frac{\hat{\boldsymbol{z}} \times \hat{\boldsymbol{x}}}{||\hat{\boldsymbol{z}} \times \hat{\boldsymbol{x}}||} \quad (1)$$

All the points can be transformed relative to frame $\{\hat{0}\}$. The reconstructed surface can be transformed back to the robot base frame after applying the interpolation.

In our proposed eABOS, the computational time is reduced and surface continuity is also guaranteed. Instead of directly interpolating the surface on a grid with the desired lattice mesh dimension d^*, a gross interpolation can be initially performed on a lattice mesh equal to d^*, λ where $\lambda > 1$ is an integer scaling factor. Once the surface has been interpolated on the gross lattice, a second fine interpolation is performed in order to improve the resolution of the lattice grid to the desired value d^*. Such a fine interpolation is achieved using the *Catmull spline patch*, as shown in Fig. 1. This guarantees continuity of C^1.

There are two major advantages of using ABOS over other surface interpolation techniques: 1) the surface can be determined given a set of unordered points, and 2) the cloud of points that describe the 3D surface are sorted into a 2D matrix. Fig. 2 shows the overall process.

B. Active Constraints for arthroscopy

A rigid instrument attached to the end effector of the manipulator is considered in this analysis. Three reference frames are introduced (Fig. 3): the first frame $\{b\} = (\boldsymbol{x}_b, \boldsymbol{y}_b, \boldsymbol{z}_b)$, has the $\boldsymbol{z}$ axis parallel to the instrument axis and the origin is centred with the proximal end of the instrument axis; the second frame, $\{c\}$, is chosen with the same orientation of the

[1]This choose of points degenerates if the plane is orthogonal to the *xy* plane.

previous one, but centred at the instrument distal tip. The third reference frame $\{a\}$ is attached to the manipulator end-effector. The homogeneous transformation matrices ${}^{i}\boldsymbol{T}_{j}$ from the reference frame $\{i\}$ to the reference frame $\{j\}$ can be trivially defined.

Whilst Virtual Fixtures constrain only the linear velocity of a laparoscopic instrument [1], a 6 × 6 impedance matrix $\boldsymbol{G}$ is introduced to relate the frame $\{b\}$ linear velocity $\boldsymbol{v}_b$ and angular velocity $\boldsymbol{\omega}_b$ with the control force $\boldsymbol{f}$ and torque $\boldsymbol{\mu}$ which are defined in Cartesian space as $[\boldsymbol{f}, \boldsymbol{\mu}]^T = \boldsymbol{G}[\boldsymbol{v}_b, \boldsymbol{\omega}_b]^T$.

Given the vector $\boldsymbol{r} = (\boldsymbol{p}_T - \boldsymbol{p}_b)$, from the origin of the $\{b\}$ frame $\boldsymbol{p}_b$ to the incision point position $\boldsymbol{p}_T$, as shown in Fig. 4, both linear and angular velocities ($\boldsymbol{v}_b$ and $\boldsymbol{\omega}_b$), of the reference frame $\{b\}$ can be decomposed into two components. Velocities $\boldsymbol{v}_{\parallel}$ and $\boldsymbol{\omega}_{\parallel}$ denote the components parallel to $\boldsymbol{r}$. The other components perpendicular to $\boldsymbol{r}$, $\boldsymbol{v}_{\perp}$ and $\boldsymbol{\omega}_{\perp}$, have to be constrained to prevent tangential motion at the incision port. The decomposition for $\boldsymbol{v}_b$ is defined below and is analogous for $\boldsymbol{\omega}_{\parallel}$ and $\boldsymbol{\omega}_{\perp}$:

$$\boldsymbol{v}_{||} = \left(\frac{\boldsymbol{r}\boldsymbol{r}^T}{||\boldsymbol{r}||^2}\right)\boldsymbol{v}_b \qquad \boldsymbol{v}_{\perp} = \boldsymbol{v}_b - \boldsymbol{v}_{||} = \left(\boldsymbol{I}_3 - \frac{\boldsymbol{r}\boldsymbol{r}^T}{||\boldsymbol{r}||^2}\right)\boldsymbol{v}_b \quad (2)$$

where $\boldsymbol{I}_3$ is the 3 × 3 identity matrix.

In order to ensure the instrument passes through the incision position, the linear velocity perpendicular to the rigid instrument direction at the incision point $\boldsymbol{v}_{RCM,\perp}$ must be *zero*. So, it is possible to define a proper angular velocity $\boldsymbol{\omega}^*$ for the component of the angular velocity such that:

$$\omega^*: \quad \boldsymbol{v}_{RCM,\perp} = \boldsymbol{v}_{\perp} + \omega^* \times \boldsymbol{r} = 0 \quad (3)$$

The component of the angular velocity $\boldsymbol{\omega}^*$ has to be perpendicular to both linear velocity $\boldsymbol{v}_{\perp}$ and unitary vector $\boldsymbol{r}$, and its module should be such that (3) is true. By introducing the 3 × 3 skew-symmetric matrix $[\boldsymbol{r}_{\times}]$ equivalent to the cross-product ($\boldsymbol{r}\times$), the angular velocity component $\boldsymbol{\omega}^*$ can be expressed as:

$$\omega^* = -\frac{||\boldsymbol{v}_{\perp}||}{||\boldsymbol{r}||}\frac{\boldsymbol{r}\times\boldsymbol{v}_{\perp}}{||\boldsymbol{r}\times\boldsymbol{v}_{\perp}||} = -\frac{1}{||\boldsymbol{r}||^2}\,[\boldsymbol{r}_{\times}]\left(\boldsymbol{I}_3 - \frac{\boldsymbol{r}\boldsymbol{r}^T}{||\boldsymbol{r}||^2}\right)\boldsymbol{v}_b \quad (4)$$

Hence, the angular velocity component $\tilde{\omega}$:

$$\tilde{\omega} = \omega_{\perp} - \omega^* = \left(\boldsymbol{I}_3 - \frac{\boldsymbol{r}\boldsymbol{r}^T}{||\boldsymbol{r}||^2}\right)\omega_b + \frac{1}{||\boldsymbol{r}||^2}\,[\boldsymbol{r}_{\times}]\left(\boldsymbol{I}_3 - \frac{\boldsymbol{r}\boldsymbol{r}^T}{||\boldsymbol{r}||^2}\right)\boldsymbol{v}_b \quad (5)$$

has to be reduced. Thus, a proportional controller can be introduced, *i.e.* $\mu = \boldsymbol{k}_{\mu}\tilde{\omega}$, where $\boldsymbol{k}_{\boldsymbol{\mu}}$ is the gain, for defining the robot control moment $\boldsymbol{\mu}$.

Apart from the RCM, the tip position also has to be constrained along the 3D surface. When the unitary surface normal $\boldsymbol{n}$ of each point is known, the linear velocity $\dot{\boldsymbol{p}}_c$ of the instrument

tip, can be decomposed into two components: one parallel to the surface $\dot{\boldsymbol{p}}_{||}$ and the other perpendicular to the surface $\dot{\boldsymbol{p}}_{\perp}$:

$$\dot{\boldsymbol{p}}_{\perp} = \left(\boldsymbol{n}\boldsymbol{n}^T\right)\dot{\boldsymbol{p}}_c \qquad \dot{\boldsymbol{p}}_{||} = \dot{\boldsymbol{p}}_c - \dot{\boldsymbol{p}}_{\perp} = \left(\boldsymbol{I}_3 - \boldsymbol{n}\boldsymbol{n}^T\right)\dot{\boldsymbol{p}}_c \quad (6)$$

Velocity $\dot{\boldsymbol{p}}_{\perp}$ is then presented as an error, since only the component $\dot{\boldsymbol{p}}_{||}$ parallel to the surface is compatible with the proposed constraint. Again, a proportional controller, *i.e.* $\boldsymbol{f}=\boldsymbol{k}_{\boldsymbol{f}}\dot{\boldsymbol{p}}_{\perp}=\boldsymbol{k}_{\boldsymbol{f}}\left(\boldsymbol{n}\boldsymbol{n}^T\right)\dot{\boldsymbol{p}}_c$ can be introduced for defining the robot control force $\boldsymbol{f}$, where $\boldsymbol{k}_{\boldsymbol{p}}$ is the controller gain. It is worth noting that linear velocity $\dot{\boldsymbol{p}}_c$ is related to the linear and angular velocity of the frame $\{b\}$ by equation $\dot{\boldsymbol{p}}_c=\boldsymbol{v}_b+\omega_b \times (L \cdot \boldsymbol{z}_b)$, where L is the length of the rigid shaft and z_b is the z axis of the frame $\{b\}$. Assuming the instrument constrained by the RCM, then $z_b \approx \boldsymbol{r}/\|\boldsymbol{r}\|$. Thus:

$$\boldsymbol{f} = \boldsymbol{k}_{\boldsymbol{f}}\left(\boldsymbol{n}\boldsymbol{n}^T\right)\boldsymbol{v}_b - \boldsymbol{k}_{\boldsymbol{f}}\frac{L}{||\boldsymbol{r}||}\left(\boldsymbol{n}\boldsymbol{n}^T\right)\left[\boldsymbol{r}_{\times}\right]\omega_b \quad (7)$$

In considering both (5) and (7), impedance matrix $\boldsymbol{G}$ is defined as:

$$\boldsymbol{G} = \begin{bmatrix} \boldsymbol{k}_{\boldsymbol{f}}\left(\boldsymbol{n}\boldsymbol{n}^T\right) & -\boldsymbol{k}_{\boldsymbol{f}}\frac{L}{||\boldsymbol{r}||}\left(\boldsymbol{n}\boldsymbol{n}^T\right)\left[\boldsymbol{r}_{\times}\right] \\ \boldsymbol{k}_{\mu}\frac{1}{||\boldsymbol{r}||^2}\left[\boldsymbol{r}_{\times}\right]\left(\boldsymbol{I}_3 - \frac{\boldsymbol{r}\boldsymbol{r}^T}{||\boldsymbol{r}||^2}\right) & \boldsymbol{k}_{\mu}\left(\boldsymbol{I}_3 - \frac{\boldsymbol{r}\boldsymbol{r}^T}{||\boldsymbol{r}||^2}\right) \end{bmatrix} \quad (8)$$

The proposed control method represents a general framework that can be applied to any back-drivable or compliant manipulator capable of providing 6 DoFs in Cartesian space. However, for a manipulator that does not provide velocity sensing, numerical differentiation has to be used for the estimation of linear and angular velocity which reduces the signal-to-noise ratio. To overcome this drawback, rather than using velocity-based constraints, the end-effector reference pose for a compliant robot is used.

The orientation constraint can be evaluated by an axis-angle rotation matrix ${}^0\boldsymbol{R}_{\boldsymbol{a}}(\alpha)$. The rotation angle $\boldsymbol{a}$ between the actual direction of the instrument denoted by z_b and the desired orientation identified by the vector $\boldsymbol{r}$ connecting $\boldsymbol{p}_T$ and $\boldsymbol{p}_b$, is equal to (Fig. 4):

$$\alpha = atan2\left(||\boldsymbol{z}_b \times \boldsymbol{r}||/||\boldsymbol{r}||, \boldsymbol{z}_b^T \cdot \boldsymbol{r}/||\boldsymbol{r}||\right) \quad (9)$$

The rotation axis a, perpendicular to both $\boldsymbol{z}_b$ and $\boldsymbol{r}$, can be defined as: $\boldsymbol{a} = \boldsymbol{z}_b \times \boldsymbol{r}/\|\boldsymbol{z}_b \times \boldsymbol{r}\|$. To constrain the tool tip position, the closest point c^* on the desired surface relative to the actual tip position can be presented as the equilibrium position for the spring behaviour of the compliant robot. Thus, the reference pose in frame $\{b\}$ can be expressed as:

$${}^0\boldsymbol{T}_{b,ref} = \begin{bmatrix} {}^0\boldsymbol{R}_{\boldsymbol{a}}(\alpha){}^0\boldsymbol{R}_b & \boldsymbol{c}^* - L\boldsymbol{z}_b \\ 0 \quad 0 \quad 0 & 1 \end{bmatrix} \quad (10)$$

where ${}^{0}\boldsymbol{R}_{b}$ is the rotation matrix of the actual pose of the robot and $-L\boldsymbol{z}_{b}$ the linear translation from the tool tip position $\boldsymbol{p}_{c}$ to the proximal end $\boldsymbol{p}_{b}$ of the rigid instrument.

C. Considerations for flexible instruments

The impedance matrix (8) can also be applied to the control of flexible instrument. The reference frame $\{c\}$ must be centred at the tip of the flexible instrument and (7) has to be slightly modified, since the relationship between the tip velocity $\dot{\boldsymbol{p}}_{c}$ and the linear $\boldsymbol{v}_{b}$ and angular $\boldsymbol{\omega}_{b}$ velocity of the $\{b\}$ frame is defined as: $\dot{\boldsymbol{p}}_{c}=\boldsymbol{v}_{b}+\omega_{b}\times(\boldsymbol{p}_{c}-\boldsymbol{p}_{b})$, where the vector $(\boldsymbol{p}_{c}-\boldsymbol{p}_{b})$ from the centre of the $\{b\}$ frame to the centre of the $\{c\}$ frame varies with the instrument configuration.

We developed a flexible instrument for arthroscopy that can be hand-held in free space or docked on to the Light Weight Robot 4+ (LWR) (KUKA Roboter, Germany) (Fig. 5). The instrument has a rigid shaft and a bendable tip that can be deflected by a pair of antagonistic tendons that terminate at the distal tip. The bendable section of the instrument is manufactured from super-elastic nitinol tube. A series of profiles are machined in one plane of the tube using electro-discharge machining (EDM). This effectively forms a 1 DoF spine that allows the tip to deflect in the plane of the profiling but also provides lateral rigidity. The antagonistic tendons are routed through the instrument shaft, back to a chassis containing the tendon drive system. The tendon drive system comprises of a pulley system, through which the tendons are routed and a capstan that pulls/releases the tendons as it is rotated by a DC motor (Faulhaber, Schonaich, Germany) through a gear train. The instrument shaft and bendable tip have an outer diameter of 6 *mm* and a 3 *mm* bore through which cameras, imaging probes and interventional devices (such as laser ablation probes) can be passed through and interchanged.

The instrument chassis is mounted on a bearing assembly within the casing, this allows a rotation DoF about the shaft axis using a second DC motor (Faulhaber) and an internal gear mounted concentric to the shaft axis.

III. Experimental Setup and Subject Tests

A minimally invasive laser chondroplasty was simulated for analysing the effects of the proposed control framework and subject tests were performed. A rigid instrument was integrated with a LWR, and the control law as presented in (10) was implemented. A knee phantom (Sawbones Europe AB, Malm, Sweden) comprised of a femur, tibia, patella, menisci and ligaments was used. A synthetic tissue representing the skin and the muscles covered these internal anatomical structures. In order to simulate the conditions of arthroscopy, the operating site was accessed through a small port created in the phantom and localised accordingly to a real scenario. Direct vision was not involved; an endoscopic camera was used to view the operating site through a second incision. The endoscope was connected with a second LWR, acting as a fixed camera holder. Visual feedback was provided to the operator through a 2D screen. The experimental setup is shown in Fig. 6.

Twelve right-handed subjects (six males, six females) were instructed to move the instrument tip along a pre-defined path within the condyles area, whilst ensuring the instrument always passed through the incision port (Fig. 7).

Each experiment was composed of three different phases in the following sequence:

1. Free motion of the instrument - A training time was given to familiarise subject with the setup;
2. Acquisition of the control points - The subject was asked to acquire five control points for reconstructing the articular surface (mean distance: 5.1 *mm*);
3. Path following - The subject attempted to move the tip as accurately as possible whilst following the path marked on the cartilage and assuring the instrument passed through the incision port.

The subjects repeated the same task twice. In the control experiment, which was conducted for comparison, the subject could freely move the instrument, whilst the robot was not constraining his/her motion. In the second experiment the robot actively constrained the orientation of the instrument in order to ensure the instrument passed through the incision port. The order of these two experiments was randomised so as to eliminate any bias due to the learning effect.

IV. Results

A. eABOS method validation

To validate the proposed surface reconstruction algorithm, a CT model of the knee phantom used in the subject tests was acquired. The surface is represented by a high-resolution mesh (41,987 Vertices; 84,092 Faces). The highlighted area in Fig. 8, which comprises 374 vertices (automatically extracted from the DICOM CT image of the phantom), was reconstructed using the eABOS technique. The CT model is considered as the ground truth. The surface reconstruction algorithm was executed 62 times. Each time the number of control points was varied, thus changing the average minimum distance δ between points. The relationship between the distance δ and the reconstruction mean error ε, *i.e.* the average distance between each point on the ground truth CT model and the closest point within the eABOS reconstructed surface, follows the trend (R^2 = 0.9343):

$$\varepsilon\ [\mu m] = 5.655\ (\delta\ [mm])^2 + 1.557\ (\delta\ [mm]) + 178.6 \quad (11)$$

Thus, for an average distance among control points equal to 5 *mm*, the reconstruction mean error is equal to 0.33 *mm*.

B. Active Constraints performances evaluation

The following performances indices were considered:

1. **Completion Time** - The time for covering the whole path;

2. **Orientation Error** - Distance between the instrument axis and the incision position. It is evaluated as the displacement between the point $\boldsymbol{p}_T$ and the line oriented as $\boldsymbol{z}_b$ and passing through $\boldsymbol{p}_b$;
3. **Intracorporeal Error**. Distance between the instrument tip position $\boldsymbol{p}_c$ and the closest point c^* within the predefined surface, as introduced in (10)[2];
4. **Extracorporeal Error**. Angle between the subject's hand position, which is assumed to be coincident with the proximal end of the laparoscopic instrument $\boldsymbol{p}_b$, and the incision point $\boldsymbol{p}_T$ around the closest point c^* (Fig. 8).
5. **Difficulty Index**. At the end of each execution, subjects were asked to evaluate qualitatively, with a score from 1 (extremely easy) to 6 (extremely difficult), the perceived difficulty in constraining the instrument orientation.

Results are quoted in Table I, and the performance enhancement is shown in Fig. 9. An increase in completion time was found when the Active Constraints technique was applied. This is a consequence of the disorientation due to the mirrored movements that have to be executed when the orientation constraint is applied. It is worth noting that no subjects have a MIS background. The reduction in the orientation error was highly statistically significant, and its mean value was reduced to about one quarter. Thus, the Active Constraints technique may lead to reduce damage to the patient's skin and tissue. The intracorporeal error is larger when constraints were applied, although this result is not statistically significant. The extracorporeal error is related to both intracorporeal and orientation errors, it is considered as a performance index of the overall system. This error is almost halved, showing a highly statistically significant enhancement in the subjects performances.

C. Flexible instrument analysis

The behaviour of the continuous bendable tip has been analysed. An Aurora Electromagnetic Measurement System (Northern Digital Inc., Ontario, CA) was used for tracking the motion of the tip whilst the DC motor was rotated at a constant speed. A 6 DoFs electromagnetic sensor was used (Aurora Mini 6DOF Sensor) and inserted through the flexible instrument. The bending angle, defined as the angle between the longitudinal axis of the instrument and the tip direction, was measured and these results are plotted in Fig. 10.

Calibration curves are different according to the motor direction, due to backlash in the tendon-driven system. The motor position-bending angle relationship is linear, with a coefficient of determination $R^2 > 0.99$ for both motion directions. Repeatability is equal to 6.9% (ANSI/ISA-51.1-1979). Measurements from the subject tests were used for evaluating the amount of surface that can be scanned with an optimal approach direction of 90° varying the bending range of motion. Results are shown in Fig. 11.

[2]The predefined surface is considered equal to the eABOS reconstructed surface, which represents a good approximation of the real surface, as proved in Subsection IV-A.

V. Conclusions

A *hands-on* collaborative control framework is introduced, in line with other orthopaedic surgical platforms such as the Acrobot or MAKOplasty. The robotic system has been developed with the purpose of providing a precise, safe and ergonomic platform for the treatment of early-stage knee arthritis. A 6 DoFs Active Constraints technique was proposed, which extended the 3 DoFs Virtual Fixtures law, for constraining an arthroscopic instrument pose during MIS. The technique represents a general control framework that can be applied to any 6 DoFs back-drivable robot. The control law was designed for incorporating a dexterous arthroscopic instrument. A surface interpolation technique for *in situ* reconstruction of anatomical surfaces was developed, which guarantees surface continuity, assuring seamless motion of the instrument without requiring pre-operative imaging, reducing the radiation dose to patients and not requiring image registration. A flexible instrument was designed for enhancing both reachable and dexterous workspace in order to increase accessibility to the target anatomy. This increased dexterity can offer improved camera views, superior positioning of imaging probes and greater cartilage ablation rates of interventional devices as the flexible tip remains perpendicular to the cartilage surface.

The subject tests results have demonstrated a statistically significant enhancement in the accuracy when the control framework is applied. Furthermore, a reduction in the perceived difficulties was recorded. The additional constraint on the tip position is expected to further reduce the intracorporeal error and consequently the extracorporeal error, enhancing the overall accuracy and safety of the procedure. The instrument configuration is not accurately predictable if the instrument collides with the surrounding anatomy. Repeatability can be software-compensated if a feedback about the instrument configuration is provided. Thus, precise shape sensing should be integrated in order to provide accurate information about the pose of the flexible instrument.

References

[1]. Bettini A, Marayong P, Lang S, et al. Vision-assisted control for manipulation using virtual fixtures. IEEE Trans. Robot. 2004; 20(6):953–966.

[2]. Yen PL, Davies BL. Active constraint control for image-guided robotic surgery. Proc Inst Mech Eng H. 2010; 224(5):623–631. [PubMed: 20718267]

[3]. Li M, Ishii M, Taylor RH. Spatial Motion Constraints Using Virtual Fixtures Generated by Anatomy. IEEE Trans. Robot. 2007; 23(1):4–19.

[4]. Jakopec M, Harris SJ, Rodriguez y Baena F, et al. The first clinical application of a “hands-on” robotic knee surgery system. Comput Aided Surg. 2001; 6(6):329–339. [PubMed: 11954064]

[5]. Kwok KW, Tsoi KH, Vitiello V, et al. Dimensionality Reduction in Controlling Articulated Snake Robot for Endoscopy under Dynamic Active Constraints. IEEE Trans. Robot. 2012; 29:15–31.

[6]. Arthritis Care - Annual Report 2010. 2010. http://www.arthritiscare.org.ukhttp://www.arthritiscare.org.uk

[7]. Hunziker EB. Articular cartilage repair: basic science and clinical progress. A review of the current status and prospects. Osteoarthr. Cartil. Jun; 2002 10(6):432–463. [PubMed: 12056848]

[8]. Takahashi T, Yamamoto H. Development and clinical application of a flexible arthroscopy system. Arthroscopy. Feb; 1997 13(1):42–50. [PubMed: 9043603]

[9]. Dario P, Carrozza MC, Marcacci M, et al. A novel mechatronic tool for computer-assisted arthroscopy. IEEE Trans. Inf. Technol. Biomed. 2000; 4(1):15–29. [PubMed: 10761770]

[10]. Schenker ML, Philippon MJ. The Role of Flexible Radiofrequency Energy Probes in Hip Arthroscopy. Tech. Orthop. 2005; 20(1):37–44.

[11]. Guthart, GS.; Salisbury, JK, Jr.. The Intuitive telesurgery system: overview and application; IEEE ICRA 2000; 2000. p. 618-621.

[12]. Madhani, AJ.; Niemeyer, G.; Salisbury, JK, Jr.. The Black Falcon: a teleoperated surgical instrument for minimally invasive surgery; IEEE/RSJ IROS 1988; 1998. p. 936-944.

[13]. Kim, D.; Kobayashi, E.; Dohi, T.; Sakuma, I. In: Dohi, T.; Kikinis, R., editors. A New, Compact MR-Compatible Surgical Manipulator for Minimally Invasive Liver Surgery; MICCAI 2002; Springer; p. 99-106.Lecture Notes in Computer Science

[14]. Stoianovici D, Cleary K, Patriciu A, et al. AcuBot: a robot for radiological interventions. IEEE Trans. Robot. Autom. 2003; 19(5):927–930.

[15]. Berkelman, P.; Ma, J. A Compact, Modular, Teleoperated Robotic Minimally Invasive Surgery System; IEEE/RAS-EMBS BioRob 2006; p. 702-707.

[16]. Rosen, J.; Lum, M.; Sinanan, M.; Hannaford, B. Raven: Developing a Surgical Robot from a Concept to a Transatlantic Teleoperation Experiment. In: Rosen, J.; Hannaford, B.; Satava, RM., editors. Surgical Robotics. Springer; 2011. p. 159-197.ch. 8

[17]. Taylor R. A Steady-Hand Robotic System for Microsurgical Augmentation. Int. J. Robot. Res. 1999; 18(12):1201–1210.

[18]. Ortmaier, T.; Hirzinger, G. Cartesian control issues for minimally invasive robot surgery; IEEE/RSJ IROS 2000; p. 565-571.

[19]. Locke, RCO.; Patel, RV. Optimal Remote Center-of-Motion Location for Robotics-Assisted Minimally-Invasive Surgery; IEEE ICRA 2007; p. 1900-1905.

[20]. Azimian, H.; Patel, RV.; Naish, MD. On constrained manipulation in robotics-assisted minimally invasive surgery; IEEE/RAS-EMBC Biorob 2010; p. 650-655.

[21]. Hagn U, Konietschke R, Tobergte A, et al. DLR MiroSurge: a versatile system for research in endoscopic telesurgery. IJCARS. 2010; 5(2):183–193.

[22]. Dressler, M. Interpolation methods for construction of surfaces [Ph.D. dissertation]. Technical University of Liberec; 2007.

[23]. Jacoby, WG. Regression III: Advanced Methods. 2005. http://polisci.msu.edu/jacoby/icpsr/regress3/http://polisci.msu.edu/jacoby/icpsr/regress3/

Europe PMC Funders Author Manuscripts

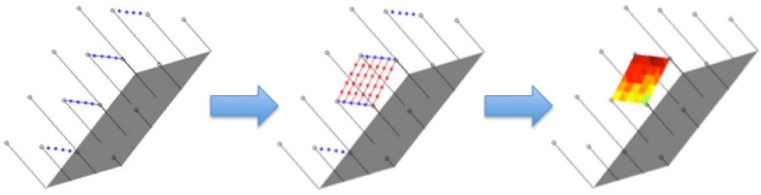

Fig. 1.

When performing the row interpolation (blue), the Catmull spline interpolation is applied row-by-row for all of the points within the convex hull of the pre-planned surface (left), thus reducing the row dimension of λ. When all the rows have been interpolated, the same process is repeated for all the columns (red, centre), thus reducing the mesh dimension to the desired value ($d^* \times d^*$) (right).

Europe PMC Funders Author Manuscripts

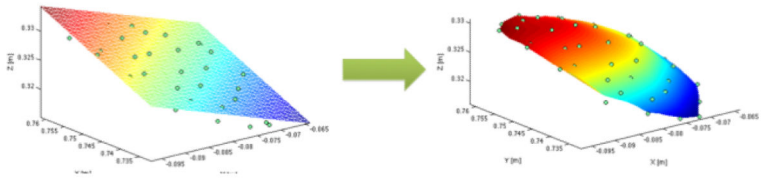

Fig. 2.

(left) Once the set of 3D control points is acquired, the multiple regression plane is evaluated; (right) After ABOS interpolation has been performed, *Catmull spline patch* interpolation is finally applied for increasing the surface resolution.

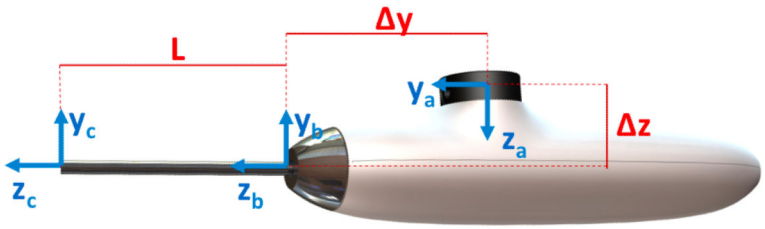

Fig. 3.
Definition of reference frames for the rigid instrument.

Europe PMC Funders Author Manuscripts

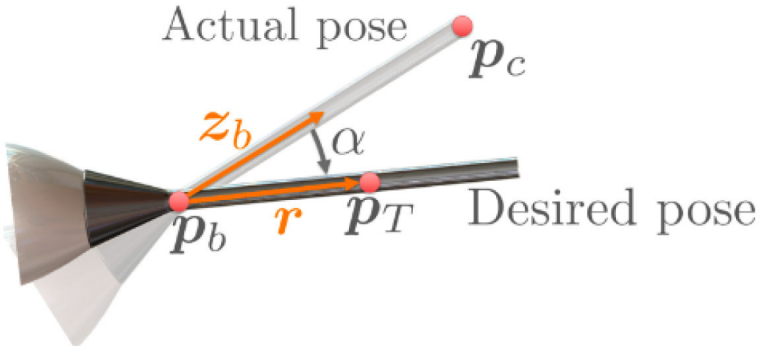

Fig. 4.

The orientation constraint is applied by rotating the instrument of angle α about the point $\boldsymbol{p}_b$ along the plane containing both $\boldsymbol{z}_b$ and $\boldsymbol{r}$.

Europe PMC Funders Author Manuscripts

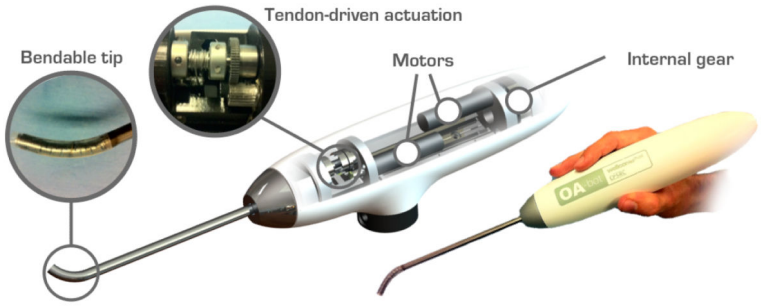

Fig. 5.

Flexible instrument for knee chondroplasty. The instrument can be connected on a positioner (such as the KUKA LWR 4+) or used standalone.

Europe PMC Funders Author Manuscripts

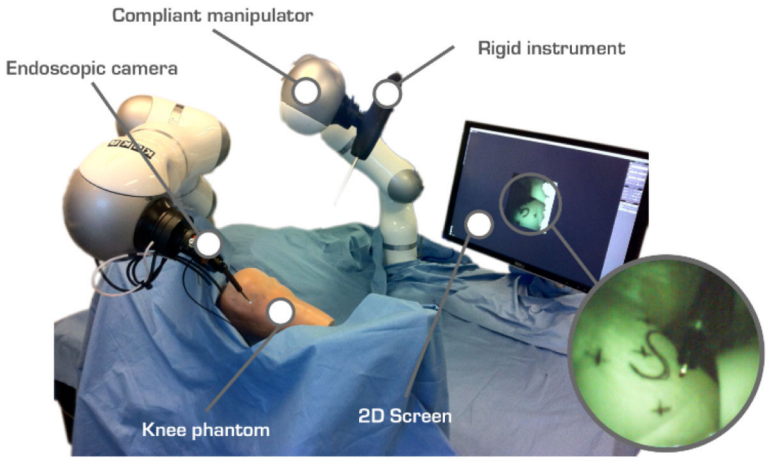

Fig. 6.

Simulated chondroplasty conducted on a knee phantom. The rigid instrument was inserted into the joint cavity through a port. The other manipulator is acting as an endoscope holder for steady visualisation on the screen.

Europe PMC Funders Author Manuscripts

Fig. 7.

An example path-following result of a subject. The subject has to draw a trajectory on the pre-defined path with and without the motion constraints.

Europe PMC Funders Author Manuscripts

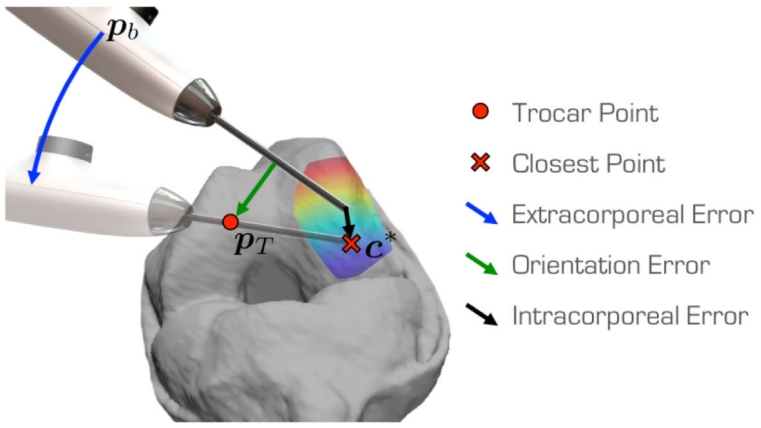

Fig. 8.

The extracorporeal error is the angular error between the actual instrument orientation, and the orientation it should have had for passing through the incision point and being in contact with the pre-defined region. The highlighted area on the CT scan represents the ground truth for the eABOS validation.

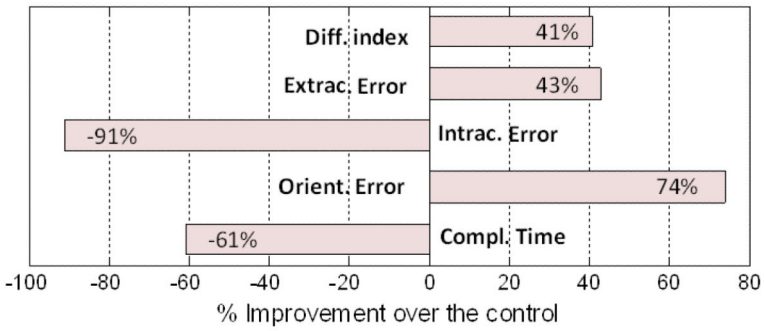

Fig. 9.

Improvement over the control hypothesis, evaluated as difference between CTRL and TEST normalised by CTRL.

Europe PMC Funders Author Manuscripts

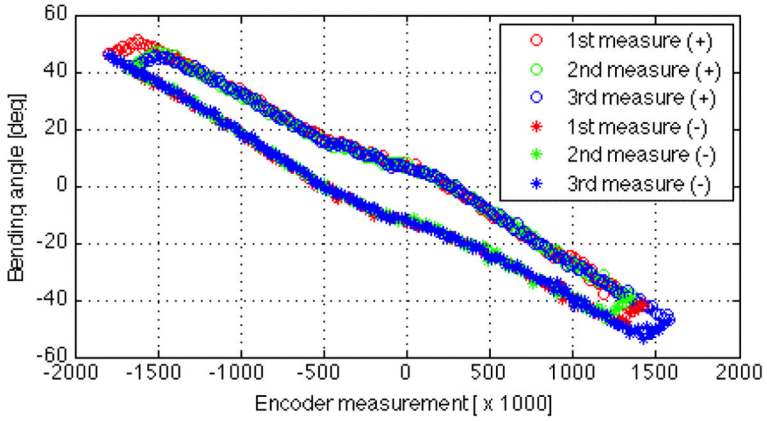

Fig. 10.

Calibration curve for the bending angle. Measurements were repeated three times for clockwise (+) and counterclockwise (−) motor motion directions.

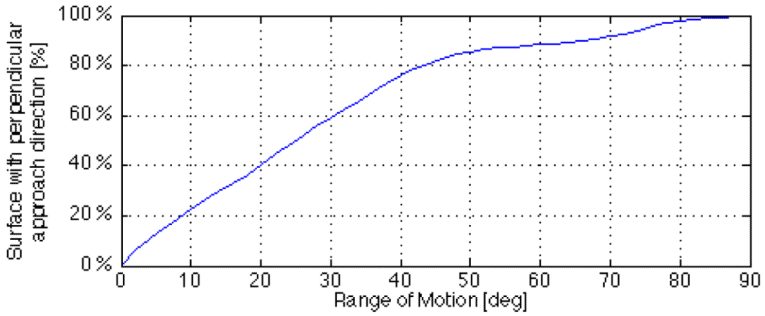

Fig. 11.

Amount of surface that can be scanned with the tip perpendicular to the articular surface varying the bending range of motion.

Europe PMC Funders Author Manuscripts

Europe PMC Funders Author Manuscripts

TABLE I

Results of the subject tests: performance indexes.

		Compl. Time [s]	Orient. Error [mm]	Intrac. Error [mm]	Extrac. Error [deg]	Diff. Index [1-6]
TEST	Mean	77.8	2.2	4.8	4.6	2.8
	SD	41.8	0.6	3.6	2.3	0.9
	Norm.[a]	> 0.05	> 0.05	> 0.05	> 0.05	0.02
CTRL	Mean	48.2	8.5	2.5	8.2	4.8
	SD	20.2	3.1	1.5	2.9	0.8
	Norm.[a]	> 0.05	> 0.05	> 0.05	> 0.05	0.03
F-Test[b]		0.02	< 0.001	0.006	> 0.05	> 0.05
p-value[c]		**0.04**	< **0.001**	> **0.05**	**0.003**	< **0.001**

[a] Normal distributions of results were tested with the Lilliefors (Kolomogrov-Smirnov) normality test. p-value is quoted.

[b] Variance equivalence F-Test. p-value is quoted.

[c] If normal distribution is met for both TEST and CTRL, the T-Test is applied; otherwise, the Wilcoxon Rank Sum Test is used.